Nakasone H, Kanda J, Yano S, Atsuta Y, Ago H, Fukuda T, Kakihana K, Adachi T, Yujiri T, Taniguchi S, Taguchi J, Morishima Y, Nagamura T, Sakamaki H, Mori T, Murata M.	A case-control study of bronchiolitis obliterans syndrome following allogeneic hematopoietic stem cell transplantation.; GVHD Working Group of the Japan Society for Hematopoietic Cell Transplantation.	Transpl Int.	26	631-9	2013
Nakasone H, Kurosawa S, Yakushijin K, Taniguchi S, Murata M, Ikegame K, Kobayashi T, Eto T, Miyamura K, Sakamaki H, Morishima Y, Nagamura T, Suzuki R, Fukuda T.	Impact of hepatitis C virus infection on clinical outcome in recipients after allogeneic hematopoietic cell transplantation.	Am J Hematol.	88	144-6	2013
Atsuta Y, Kanda J, Takanashi M, Morishima Y, Taniguchi S, Takahashi S, Ogawa H, Ohashi K, Ohno Y, Onishi Y, Aotsuka N, Nagamura-Inoue T, Kato K, Kanda Y.	Different effects of HLA disparity on transplant outcomes after single-unit cord blood transplantation between pediatric and adult patients with leukemia.	Haematologica.	98	814-22	2013
Yamamoto S, Ebihara Y, Mochizuki S, Kawakita T, Kato S, Ooi J, Takahashi S, Tojo A, Yusa N, Furukawa Y, Oyaizu N, Watanabe J, Sato K, Kimura F, Tsuji K.	Quantitative PCR detection of CEP110-FGFR1 fusion gene in a patient with 8p11 syndrome (letter to the editor).	Leuk Lymphoma.	4(9)	2068-9	2013

Ishiyama K, Takami A, Kanda Y, Nakao S, Hidaka M, Maeda T, Naoe T, Taniguchi S, Kawa K, **Nagamura T**, Tabuchi K, Atsuta Y, Sakamaki H.	Prognostic factors for acute myeloid leukemia patients with t(6;9)(p23;q34) who underwent an allogeneic hematopoietic stem cell transplant.	Leukemia	26	1416-9	2013
Kurosawa S, Yakushijin K, Yamaguchi T, Atsuta Y, **Nagamura-Inoue T**, Akiyama H, Taniguchi S, Miyamura K, Takahashi S, Eto T, Ogawa H, Kurokawa M, Tanaka J, Kawa K, Kato K, Suzuki R, Morishima Y, Sakamaki H, Fukuda T.	Changes in incidence and causes of non-relapse mortality after allogeneic hematopoietic cell transplantation in patients with acute leukemia/myelodysplastic syndrome: an analysis of the Japan Transplant Outcome Registry.	Bone Marrow Transplant.	48(4)	529-36	2013

TISSUE ENGINEERING: Part B
Volume 20, Number 3, 2014

DOI: 10.1089/ten.teb.2013.0578

The Use of Bone Marrow Stromal Cells (Bone Marrow-Derived Multipotent Mesenchymal Stromal Cells) for Alveolar Bone Tissue Engineering: Basic Science to Clinical Translation

Hideaki Kagami, DDS, PhD,[1–3] Hideki Agata, DDS, PhD,[4] Minoru Inoue, DDS, PhD,[1,2] Izumi Asahina, DDS, PhD,[4] Arinobu Tojo, MD, PhD,[1] Naohide Yamashita, MD, PhD,[2] and Kohzoh Imai, MD, PhD[5]

Bone tissue engineering is a promising field of regenerative medicine in which cultured cells, scaffolds, and osteogenic inductive signals are used to regenerate bone. Human bone marrow stromal cells (BMSCs) are the most commonly used cell source for bone tissue engineering. Although it is known that cell culture and induction protocols significantly affect the *in vivo* bone forming ability of BMSCs, the responsible factors of clinical outcome are poorly understood. The results from recent studies using human BMSCs have shown that factors such as passage number and length of osteogenic induction significantly affect ectopic bone formation, although such differences hardly affected the alkaline phosphatase activity or gene expression of osteogenic markers. Application of basic fibroblast growth factor helped to maintain the *in vivo* osteogenic ability of BMSCs. Importantly, responsiveness of those factors should be tested under clinical circumstances to improve the bone tissue engineering further. In this review, clinical application of bone tissue engineering was reviewed with putative underlying mechanisms.

Introduction

ATROPHIC ALVEOLAR BONE is one of the major obstacles for dental implant therapy and there are a large number of patients without sufficient bone volume. For patients with severe bone atrophy, autologous bone grafts have been performed.[1] However, even the amount of harvesting bone is small, the procedure is accompanied by swelling and pain of the donor site.[2] Although bioartificial bone substitutes have been frequently used, the ability to induce bone is limited.[3] Accordingly, less invasive and more efficient bone regeneration therapy is awaited, such as tissue engineering.

The first results of clinical bone tissue engineering were published in 2001.[4] In this study, the regeneration of long bone defects was tested using hydroxyapatite blocks together with cultured autologous bone marrow stromal cells (BMSCs). This tissue engineering-based approach proved the feasibility of this concept. The results from a preliminary clinical study of alveolar bone regeneration were published thereafter.[5] In this review, studies on clinical alveolar bone tissue engineering are summarized. Then, the problems associated with current tissue engineering were also discussed.

Bone Tissue Engineering and Stem Cells

Cells are considered as a major component of tissue engineering. Although the role of transplanted cells during bone tissue regeneration is still controversial, it has been proved that the transplanted cells could survive, proliferate, and differentiate into osteogenic phenotype.[6] There is accumulating evidence that the level and quality of regeneration is affected by the ability of transplanted cells.[7] Accordingly, it is important to establish an optimal cell culture protocol to maximize the function of osteogenic cells. Surprisingly, the BMSC ability to differentiate into osteoblast-like cells is easily diminished during passage and no bone formation was observed after several passages (Fig. 1).[7,8] Furthermore, cell seeding density and the period of induction also affect *in vivo* osteogenic ability. It has been

[1]Tissue Engineering Research Group, Division of Molecular Therapy, The Advanced Clinical Research Center, The Institute of Medical Science, The University of Tokyo, Tokyo, Japan.
[2]Department of Advanced Medical Science, Clinic for Bone Regeneration, IMSUT Hospital, The Institute of Medical Science, The University of Tokyo, Tokyo, Japan.
[3]Department of Oral and Maxillofacial Surgery, Matsumoto Dental University Dental School, Shiojiri, Japan.
[4]Unit of Translational Medicine, Department of Regenerative Oral Surgery, Nagasaki University Graduate School of Biomedical Sciences, Nagasaki, Japan.
[5]Center for Antibody and Vaccine, IMSUT Hospital, The Institute of Medical Science, The University of Tokyo, Tokyo, Japan.

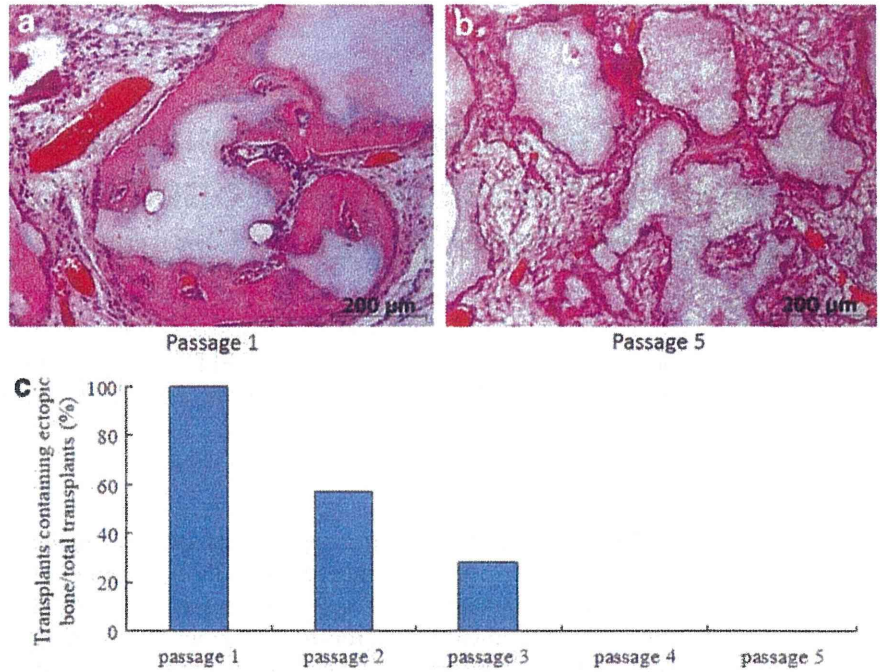

FIG. 1. Effect of passage number on ectopic *in vivo* osteogenic ability. Upper panels showing ectopic bone formation at the back of nude mice with tissue-engineered bone using passage 1 (**a**) and passage 5 (**b**) human bone marrow stromal cells (BMSCs). The success of ectopic bone formation quickly decrease after passage and no bone formation was observed after passage 4 (**c**). Note that the ability is quickly lost during passage. Modified from Agata *et al.*[7] Color images available online at www.liebertpub.com/teb

shown that basic fibroblast growth factor (bFGF) is beneficial to maintain *in vivo* osteogenic ability of BMSCs.[7]

Clinical Studies on Alveolar Bone Tissue Engineering

The results from clinical studies on alveolar bone tissue engineering using BMSCs were first reported in 2004. In this study, bone marrow-derived MSCs were mixed with platelet-rich plasma as a scaffold.[8] Bone regeneration was observed in all moderate atrophy cases. Another clinical study utilized BMSCs and hydroxyapatite granules. BMSCs were induced into osteogenic cells for 1 week and transplanted. In this study, bone formation was observed in three cases, but there was no apparent bone formation from the

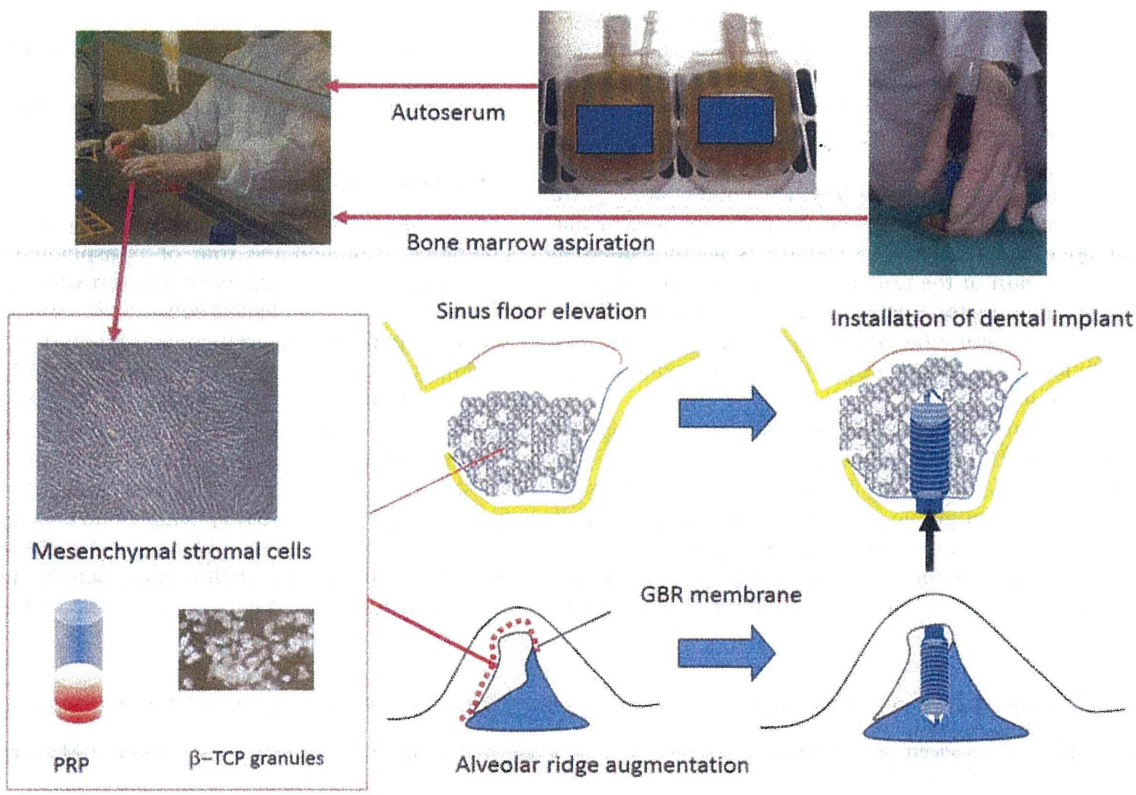

FIG. 2. The procedure for clinical study of alveolar bone regeneration at IMSUT Hospital, The Institute of Medical Science, The University of Tokyo. β-TCP, beta-tricalcium phosphate; PRP, platelet rich plasma. Color images available online at www.liebertpub.com/teb

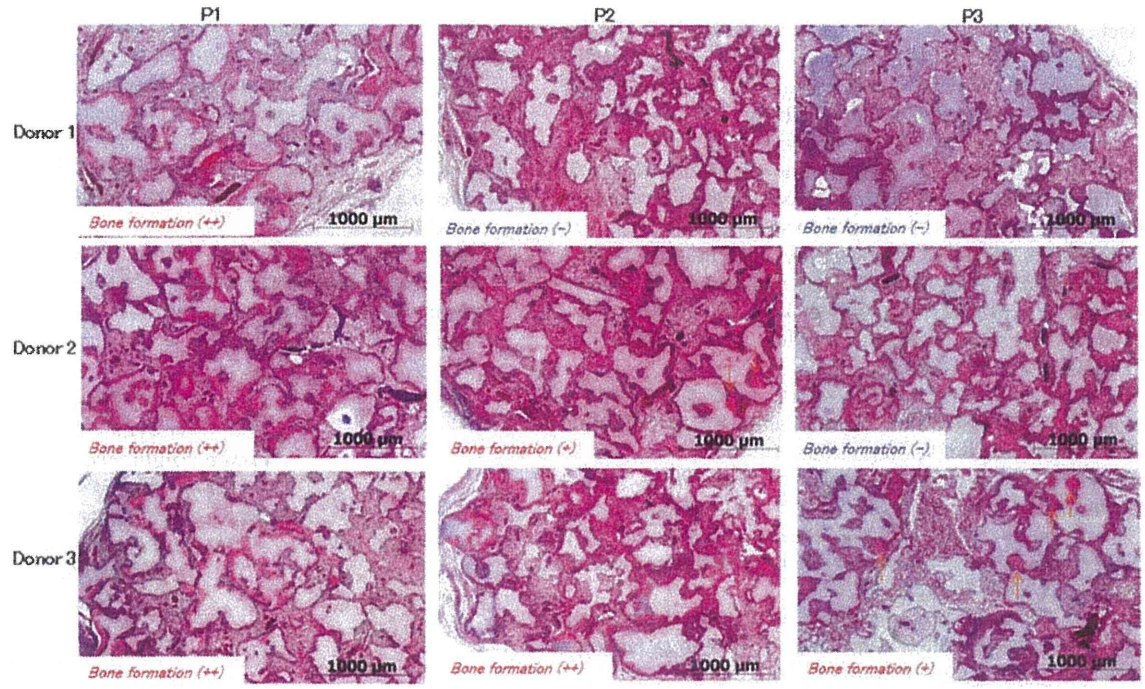

FIG. 3. Individual (donor) variations of *in vivo* osteogenic ability and their changes during passage. Note that the effect of passage differed between individuals. Modified from Agata.[9] Color images available online at www.liebertpub.com/teb

transplanted cells in cases where the atrophy was severe. Thus, the efficacy of clinical alveolar bone tissue engineering for severe atrophy cases remains controversial.

We have conducted a clinical study of bone tissue engineering for severe atrophy of alveolar bone. In this study, autologous BMSCs were transplanted together with platelet-rich plasma gel and beta-tricalcium phosphate (β-TCP) granules as scaffolds (Fig. 2). The results from a 2-year observation showed that bone regeneration was observed in all patients, although significant individual variations in cell growth, differentiation, and levels of bone regeneration were observed (Asahina *et al.*, manuscript in preparation). This type of study, focused on severe atrophy cases, may prove the usefulness of alveolar bone tissue engineering. In terms of safety, no side effects or related complications have been reported, which may imply the relatively safety nature of alveolar bone tissue engineering using BMSCs.

Toward the Establishment of Reliable Alveolar Bone Tissue Engineering Using BMSCs

Although clinical studies have confirmed the feasibility and safety of alveolar bone tissue engineering using BMSCs, one of the important clinical benchmarks is the efficacy for severe atrophy cases. The results from focused studies with selected cases will provide the evidence. Another important problem is the individual variation as shown by basic and preliminary clinical studies. Since the shape and the size of bone defect vary among individuals, it might be impossible to completely eliminate such variations. Accordingly, it should be important to minimize the variation in other factors, such as cells. In terms for BMSCs, there was no significant difference in the expression of mesenchymal stem cell markers during passage.[7] In contrast, a large variation was observed in the *in vivo* bone forming ability among donors and during passage (Fig. 3).[7,8,9] We believe the usage of early passage cells as well as growth factors (bFGF) may minimize the variation, which should be tested under clinical settings.

In spite of the number of studies and the clinical efficacy of bone tissue engineering, it is not a standard treatment at present. It is necessary to show the superiority of clinical outcome compared with standard autologous bone transplantation and allogenic (or xenogenic) transplantation. Furthermore, tissue engineering requires special facility for cell culture and there is a requirement for many safety examinations, which may also increase the cost for treatment. Those technologies, which may support the widespread use of bone tissue engineering, should be investigated.

Tissue engineering is one of the most rapidly progressing fields and alveolar bone is still an attractive target for tissue engineering.[10] The application of bone tissue engineering is not limited for dental implants and is successfully applied for other diseases such as nonunion fractures[11] and alveolar clefts.[12,13]

Disclosure Statement

No competing financial interests exist.

References

1. Jensen, S.S., and Terheyden, H. Bone augmentation procedures in localized defects in the alveolar ridge: clinical results with different bone grafts and bone-substitute materials. Int J Oral Maxillofac Implants **24 Suppl,** 218, 2009.
2. Clavero, J., and Lundgren, S. Ramus or chin grafts for maxillary sinus inlay and local onlay augmentation: comparison of donor site morbidity and complications. Clin Implant Dent Relat Res **5,** 154, 2003.

3. Becker, W., Urist, M., Becker, B.E., Jackson, W., Parry, D.A., Bartold, M., Vincenzzi, G., De Georges, D., and Niederwanger, M. Clinical and histologic observations of sites implanted with intraoral autologous bone grafts or allografts. 15 human case reports. J Periodontol **67,** 1025, 1996.
4. Quatro, R., Mastrogiacomo, M., and Cancedda, R. Repair of large bone defects with the use of autologous bone marrow stromal cells. N Engl J Med **344,** 385, 2001.
5. Yamada, Y., Ueda, M., Hibi, H., and Nagasaka, T. Translational research for injectable tissue-engineered bone regeneration using mesenchymal stem cells and platelet-rich plasma: from basic research to clinical case study. Cell Transplant **13,** 343, 2004.
6. Meijer, G.J., de Bruijn, J.D., Koole, R., and van Blitterswijk, C.A. Cell based bone tissue engineering in jaw defects. Biomaterials **29,** 3053, 2008.
7. Agata, H., Asahina, I., Watanabe, N., Ishii, Y., Kubo, N., Ohshima, S., Yamazaki, M., Tojo, A., and Kagami, H. Characteristic change and loss of *in vivo* osteogenic abilities of human bone marrow stromal cells during passage. Tissue Eng Part A **16,** 663, 2010.
8. Sugiura, F., Kitoh, H., and Ishiguro, N. Osteogenic potential of rat mesenchymal stem cells after several passages. Biochem Biophys Res Commun **316,** 233, 2004.
9. Agata, H. Toward establishment of truly reliable protocol for bone tissue Engineering. Regenerative Medicine, **8,** 439, 2009. (In Japanese).
10. Egusa, H., Sonoyama, W., Nishimura, M., Atsuta, I., and Akiyama, K. Stem cells in dentistry—Part II: clinical applications. J Prosthodont Res **56,** 229, 2012.
11. Shoji, T., Ii, M., Mifune, Y., Matsumoto, T., Kawamoto, A., Kwon, S.M., Kuroda, T., Kuroda, R., Kurosaka, M., and Asahara, T. Local transplantation of human multipotent adipose-derived stem cells accelerates fracture healing via enhanced osteogenesis and angiogenesis. Lab Invest **90,** 637, 2010.
12. Pradel, W., and Lauer, G. Tissue-engineered bone grafts for osteoplasty in patients with cleft alveolus. Ann Anat **194,** 545, 2012.
13. Janssen, N.G., Weijs, W.L., Koole, R., Rosenberg, A.J., and Meijer, G.J. Tissue engineering strategies for alveolar cleft reconstruction: a systematic review of the literature. Clin Oral Investig **18,** 219, 2014.

Address correspondence to:
Hideaki Kagami, DDS, PhD
Tissue Engineering Research Group
Division of Molecular Therapy
The Advanced Clinical Research Center
The Institute of Medical Science
The University of Tokyo
4-6-1 Shirokanedai
Minato-ku
Tokyo 108-8639
Japan

E-mail: kagami@ims.u-tokyo.ac.jp

Received: September 15, 2013
Accepted: January 30, 2014
Online Publication Date: March 5, 2014

ARTICLE

BIOTECHNOLOGY and BIOENGINEERING

Characterization of Time-Course Morphological Features for Efficient Prediction of Osteogenic Potential in Human Mesenchymal Stem Cells

Fumiko Matsuoka,[1] Ichiro Takeuchi,[2] Hideki Agata,[3] Hideaki Kagami,[3,4] Hirofumi Shiono,[5] Yasujiro Kiyota,[5] Hiroyuki Honda,[1] Ryuji Kato[1,6]

[1]Department of Biotechnology, Graduate School of Engineering, Nagoya University, Furo-cho, Chikusa-ku, Nagoya, Aichi 464-8603, Japan; telephone: +81-52-747-6811; fax: +81-52-747-6813; e-mail: kato-r@ps.nagoya-u.ac.jp

[2]Department of Engineering, Nagoya Institute of Technology, Gokiso-cho, Showa-ku, Nagoya, Aichi 466-8555, Japan

[3]Tissue Engineering Research Group, Division of Molecular Therapy, The Institute of Medical Science, The University of Tokyo, Minato-ku, Tokyo 108-8639, Japan

[4]Department of Oral and Maxillofacial Surgery, Matsumoto Dental University School of Dentistry, Hirooka, Shiojiri 399-0781, Japan

[5]Nikon Corporation, Chiyoda-ku, Tokyo 100-8331, Japan

[6]Department of Basic Medicinal Sciences, Graduate School of Pharmaceutical Sciences, Nagoya University, Furo-cho, Chikusa-ku, Nagoya, Aichi 464-8601, Japan

ABSTRACT: Human bone marrow mesenchymal stem cells (hBMSCs) represents one of the most frequently applied cell sources for clinical bone regeneration. To achieve the greatest therapeutic effect, it is crucial to evaluate the osteogenic differentiation potential of the stem cells during their culture before the implantation. However, the practical evaluation of stem cell osteogenicity has been limited to invasive biological marker analysis that only enables assaying a single end-point. To innovate around invasive quality assessments in clinical cell therapy, we previously explored and demonstrated the positive predictive value of using time-course images taken during differentiation culture for hBMSC bone differentiation potential. This initial method establishes proof of concept for a morphology-based cell evaluation approach, but reveals a practical limitation when considering the need to handle large amounts of image data. In this report, we aimed to scale-down our proposed method into a more practical, efficient modeling scheme that can be more broadly implemented by physicians on the frontiers of clinical cell therapy. We investigated which morphological features are critical during the osteogenic differentiation period to assure the performance of prediction models with reduced burden on image acquisition. To our knowledge, this is the first detailed characterization that describes both the critical observation period and the critical number of time-points needed for morphological features to adequately model osteogenic potential. Our results revealed three important observations: (i) the morphological features from the first 3 days of differentiation are sufficiently informative to predict bone differentiation potential, both activities of alkaline phosphatase and calcium deposition, after 3 weeks of continuous culture; (ii) intervals of 48 h are sufficient for measuring critical morphological features; and (iii) morphological features are most accurately predictive when early morphological features from the first 3 days of differentiation are combined with later features (after 10 days of differentiation).

Biotechnol. Bioeng. 2014;9999: 1–10.

KEYWORDS: image-based analysis; mesenchymal stem cell; non-invasive analysis; osteogenic differentiation; prediction

This article was published online on 30 January 2014. Subsequently, it was determined that the article contained an earlier version of Figure 4, and the correct version was published on 21 February 2014

Fumiko Matsuoka and Ichiro Takeuchi contributed equally to this work.

Correspondence to: R. Kato

Contract grant sponsor: New Energy and Industrial Technology Development Organization

Contract grant number: 09C46036a

Received 26 August 2013; Revision received 21 October 2013; Accepted 7 January 2014

Accepted manuscript online xx Month 2014;

Article first published online in Wiley Online Library (wileyonlinelibrary.com).

DOI 10.1002/bit.25189

Introduction

At present, the regenerative medicine market is still limited when one considers its potential impact on clinical practice. Currently, technological developments for commercial advancement of regenerative medicine are focused on cell culture automation technologies. For the purpose of industrialization, higher expectations for standardization

are now required for automation technology; platforms need to improve both quality of results and cost effectiveness (Ratcliffe 2011; Smith 2012). Recently, advances in novel imaging technologies, used to support image-based cell evaluation, have improved performance to the point where quantitative evaluation of detailed cellular events is now possible (Becker and Madany, 2012; Erdmann et al., 2012; Hong et al., 2006; Kino-oka et al., 2009; Li et al., 2010; Platt et al., 2009; Poirier-Quinot et al., 2010; Seiler et al., 2012; Unadkat et al., 2012). Non-destructive imaging methods have shown particular compatibility with cell therapy, which requires intact cells for therapy during and after their evaluations. The historical use of microscopy for cell quality evaluation suggests that morphological parameters can empirically define cell quality, but to-date no objective morphometric criteria have been directly linked to osteogenic potential (Maul et al., 2011; Platt et al., 2009; Seiler et al., 2012; Wang et al., 2013; Zhang and Kilian, 2013).

By focusing on cellular morphological information, we previously reported a non-invasive cell quality evaluation method for predicting the osteogenic differentiation potential of human bone marrow-derived mesenchymal stem cells (hBMSCs), by using only time-course collected phase contrast images (Matsuoka et al., 2013). The clinical utility of our proposed method improves upon previous reports by more accurately predicting osteogenic potential. Also, our experimental framework is designed to overcome common biases of conventional morphology-/image-based cell quality analysis approaches by satisfying three essential criteria for obtaining high-performance models: (i) timely information extracted from precisely timed image capture, assured by a fully scheduled image acquisition system; (ii) unbiased information described by carefully selected features, which are not interdependent, thereby eliminating researcher subjectivity biases; and (iii) reliable information described by features derived from sampling statistically relevant numbers of cells.

Our proposed image-based cell quality prediction presents a significant technological advancement that offers several advantages over conventional measures of hBMSC differentiation potential. Conventional differentiation markers can only be measured once, when differentiation is complete. Our proposed non-destructive method preserves all cells, which maximizes the amount of viable material for therapeutic use. Our approach also allows the continuous evaluation of the same cells from the first day to the final day. The ability to repeat measurements on the same cell population provides a greater opportunity to accurately predict optimal timing for use of the cells. An image-based cell quality assessment tool can offer new choices for clinical physicians to supply additional quality assurances for the production of cells for therapy. Especially with their heterogenic diversity of stem cells, the image-based evaluation, which measures every single cell in the culture vessel, can be a powerful tool for total cell evaluation.

However, our proposed method left some tasks to be solved for more practical usage to satisfy both the efficacy and the profitability. Since proposing the original method, we re-evaluated the large collected data set consisting of 9,990 images covering 14 days (8 h intervals) of the differentiation period. We considered that the image-dense data required to implement our method may pose a potential obstacle for clinical implementation. A fully automatic image acquisition system to support image data analysis is not always a justifiable investment for clinics performing the latest cell therapies. In facilities already performing clinical research with established standard operating procedures, changing an automated sample handling system is also not always feasible. Physical space is another limiting consideration when introducing an automation platform into a clinical environment. Therefore, to make our proposed method more widely available, we aimed to breakdown, simplify and refine the prediction scheme into a practical, resource-efficient application without losing performance. We also considered the resource demands when re-evaluating our original method: (i) the worker time involved in each image acquisition, (ii) the additional costs to fund operators for timed images at night and on weekends, (iii) the frequency and cost of occupying and maintaining the defined area (such as clean rooms), (iv) the effort of scheduling operators and space to obtain image data, and (v) the expense of purchasing, labor and maintenance of image storage media. Based on the weight of these considerations, we investigated the minimum image acquisition conditions to assure high prediction performance if our method was implemented using manual procedures rather than fully automated. In this work, we launched our investigation of constructing high-quality, resource-efficient hBMSC prediction models by aiming to define essential morphology parameters. To achieve this aim, we vetted two aspects of the information derived from cellular images during osteogenic differentiation: (i) the critical period for defining cell quality by their morphological features, and (ii) the optimal density of morphological information while retaining prediction performance. To our knowledge, there has been no detailed analysis that critically weighs the content of cellular images for the purpose of informing cell quality predictions based on cellular morphology. Since manual observation of cellular morphology has historically supported cell production, a detailed characterization of morphological characteristics over a period of time should yield deeper insights into the prediction sensitivity, and also the biological meaning of morphology-based decisions executed by cell biologists.

In this study, we used three types of algorithm modification for the characterization of morphological features: (i) shortening type: dataset characterization where the inclusion rate of morphological features along a time-line is shortened; (ii) window-shift type: dataset characterization where the inclusion period for morphological features is changed along a time-line; and (iii) skipping type: dataset characterization where the density of morphological features is reduced by decreasing time-point sampling frequency. By comparing changes in each type of model's prediction performance, we could define the sensitivity of morphological signals for

detecting collapse of hBMSC differentiation potential. We also defined the most resource-effective scheme to collect the morphological parameters to predict osteogenic differentiation potential. Our data shows not only the key conditions for feasible implementation of our proposed method by clinical physicians, but also the modeling approach that maximally satisfies both quality and efficiency of image-based cell quality prediction modeling.

Materials and Methods

Cells and Culture

Three lots of human bone marrow which were derived mesenchymal stem cells (hBMSCs) (Lonza Walkersville, Inc., Walkersville, MD) were designated as Lot 1 (strain number 15000-1, unknown race, Male, 19-year-old), Lot 2 (strain number 17174, Oriental, Male, 20-year-old), Lot 3 (strain number 11533, Black, Male, 22-year-old). Groups of cells with different passage number were prepared by expanding three lots of hBMSCs in growth medium (passage 3–5 for lot 1 and 2, passage 6–8 for lot 3) based on the clinical jaw bone therapy protocol used by our group (Kagami et al., 2011). The previously described osteogenic differentiation protocol was simultaneously applied to these cells and images acquired in parallel (detailed protocol described in Matsuoka et al., 2013). Briefly, as indicated in Figure 1, cells were seeded at a density of 1.0×10^4 cells/well in 12-well plate (Greiner Bio-One, Frickenhausen, Germany), and the cell-seeding day was designated as day 0 and cultured for expansion from days 4 to 0 in α-modified Eagle's medium (αMEM) containing 10% fetal bovine. From days 1 to 14, cells were divided into two

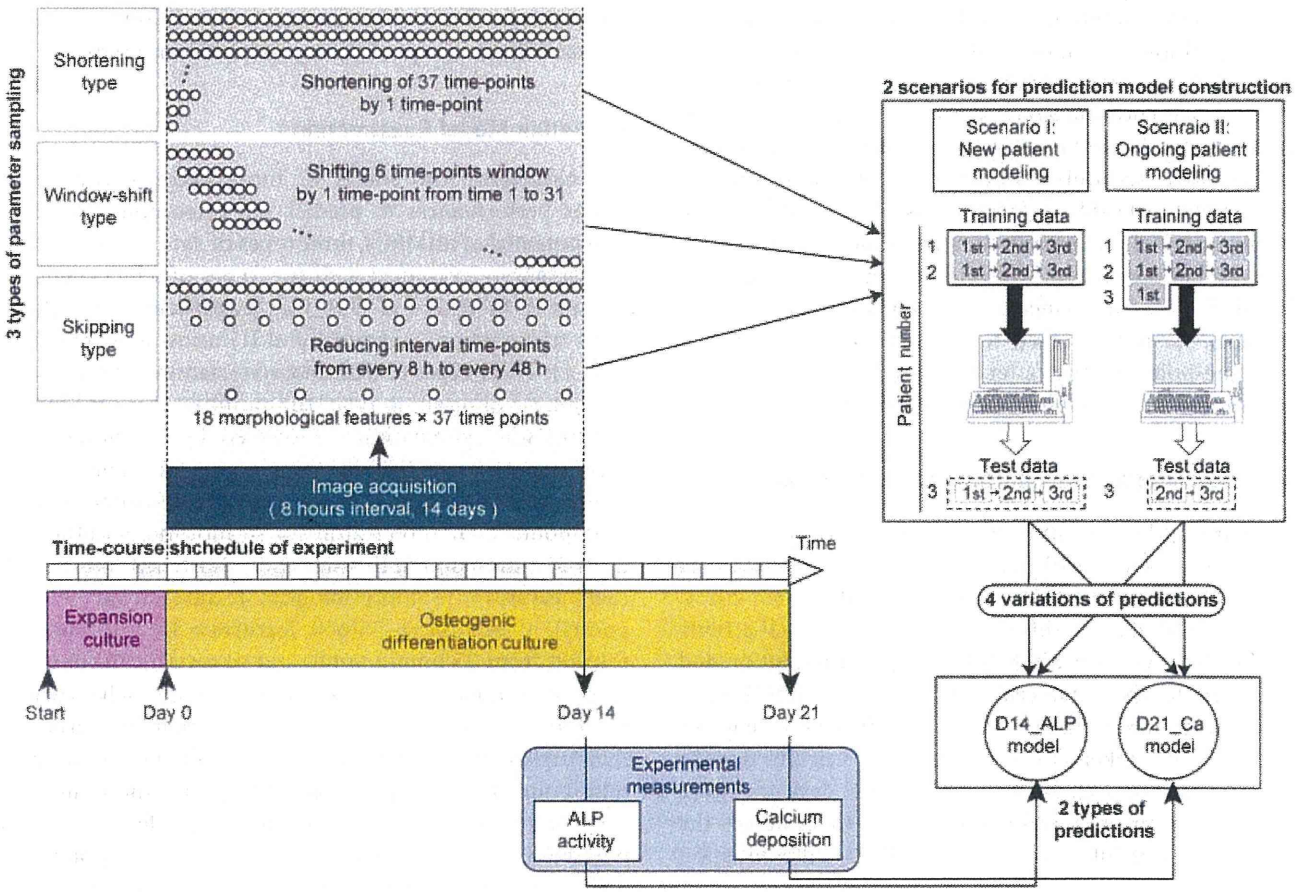

Figure 1. Schematic illustration of experimental procedures for constructing morphology-based prediction models for osteogenic differentiation potential. In the time-course experiment, an osteogenic differentiation culture period (21 days) followed the expansion culture period (4 days). For the first 14 days of differentiation culture phase contrast microscopic images were automatically acquired at 8 h intervals (total 37 time-points) using BioStation CT (Nikon). From acquired images, morphological features were extracted through image processing (total 666 morphological features). Three types of feature variation were compared: (i) Shortening type, a systematic examination of the impact of decreasing the overall duration of the experimental time-line; (ii) Window-shift type, a 6-time-point scan of the 14 day time-course to explore the possibility of a critical time window; and (iii) Skipping type, an evaluation of the critical sampling frequency between time-points. Circles in the upper-left panel represent image collection time-points. On day 14, samples were collected for experimental measurement of ALP activity. On day 21, samples were collected for calcium deposition measurement. The model predicting ALP activity on day 14 was designated as D14_ALP, and the model predicting calcium deposition rate on day 21 was designated as D21_Ca. For both prediction models, two different scenarios for model construction were examined. Scenario I: New patient modeling, which attempted to predict a new patients cell potential from historical image data of previous patients, and Scenario II: Ongoing patient modeling, which attempted to predict new patients cell potential by combining the historical image data of previous patients together with the patients own image data from early culture stages.

groups: (i) osteogenic-induction group (Induction, N = 6) and (ii) non-induction group (Control, N = 6). For the Induction group, the medium was switched to induction medium consisting of 10% FBS-containing αMEM medium supplemented with 10 nM dexamethasone (Sigma-Aldrich Corp., St. Louis, MO), 100 mM ascorbic acid (Wako Pure Chemical Industries, Ltd., Osaka, Japan), and 10 mM glycerol 2-phosphate sodium salt hydrate (Sigma-Aldrich Co.). For the non-induction group, no supplements were added to the αMEM medium containing 10% FBS. The medium was refreshed at days 3 and 9. For half of the samples in each experimental group (N = 3), alkaline phosphatase (ALP) activity was quantified on day 14, and for the rest (N = 3), calcium deposition was quantified on day 21.

Image Acquisition

During the osteogenic differentiation culture period, phase contrast microscopic images of hBMSCs were obtained using the BioStation CT (Nikon Co., Tokyo, Japan). Five view fields (center position and four positions at 2.2 mm from the center) of phase contrast images were acquired from each well at 8 h intervals covering 8 h (first image acquisition) to 320 h (last image acquisition) covering a total of 14 days. Among all 40 time-points scheduled, three time-points were omitted from analysis. Data at 8 h was omitted since the cells were not yet fully settled. Data at time 64 h and time 216 h were also omitted, since the image acquisition schedule conflicted with scheduled medium changes. As a consequence of these omissions, we re-numbered the retained data sequentially from time-point 1 (16 h after the differentiation start) to time-point 37 (320 h after the differentiation start).

Quantification of Osteogenic Differentiation Rates

Quantitative ALP activity and calcium deposition assays, which are conventional destructive experiments, were performed as previously described (Matsuoka et al., 2013). Briefly, after 14 days of differentiation culture, ALP activity was measured with a p-nitrophenyl phosphate solution and normalized to the total cell number. Since ALP activity measurement has been known as insufficient osteogenic differentiation marker in the clinical trials, calcium deposition was also measured after an additional 7 days of culture using an alizarin red staining method, to enhance the meaning of quantification of osteogenic differentiation potential.

Cell Image Processing

Cell image processing was performed as described in our previous reports (Matsuoka et al., 2013; Sasaki et al., 2013). Briefly, all images were processed using MetaMorph software (Molecular Devices, Sunnyvale, CA) with the original filter sets. After binarization, the following nine morphological features of all cellular objects in each image were measured: (i) breadth, (ii) elliptical form factor, (iii) fiber breadth, (iv) fiber length, (v) hole area, (vi) inner radius, (vii) relative hole area, (viii) shape factor, and (ix) total area. For each parameter, the average (AVE) and standard deviation (SD) of five view fields, consisting of about 4,000–40,000 cells, were calculated, yielding 18 features (consist of AVE and SD for nine features). Such AVE and SD information encompassing the time-course of 38-time-points are assigned to describe the statistical changes that arise in heterogenic group of cells. The final total features consisted of 666 features (18 morphological features within each of 37 time-points). From all of these parameters, key features were selected using the three types of dataset characterization described in the Construction and prediction models section. Morphological features were directly associated with the morphological measurement data, which were experimentally determined values, resulting in 54 samples (3 lots × 2 induction conditions × 3 passages × 3 wells) assigned with corresponding ALP values, and 54 samples assigned with calcium deposition values. This process linked the biological measurement with morphometric information to complete a dataset for use in prediction model construction.

Prediction Model Construction

To characterize the effects of morphological features on model performances to predict the osteogenic differentiation potential of hBMSCs, three types of data characterization concepts were examined with two types of target prediction models (D14_ALP and D21_Ca) constructed through two types of scenarios (scenario I and II) using ridge regression (Fig. 1). Three types of data characterization were defined as follows: (i) Shortening type: the number of morphological features was systematically decreased by 1 time-point for each sampling event along the time-course. For example, morphological features used for the full time-course included time-points 1–37 (666 features = 18 morphological features from 37 time-points); this was then shortened to time 1–36 (648 features = 18 morphological features from 36 time-points), then time 1–35(630 features = 18 morphological features from 35 time-points), and so on. (ii) Window-shift type: the number of time-points within an analysis set was fixed to 6 time-points (covering approximately 2 days), and their capture period was shifted along the time-course with 1 time-point. For example, beginning from time-point 1 the first 108 features (i.e., 18 morphological features × time-points 1–6) were included; beginning from time-point 2, the next time-matched 108 features were included (i.e., 18 morphological features × time-points 2–7), repeated to the final time-point. (iii) Skipping type: the number of morphological features included was decreased by increasing the time-point span by 8 h intervals. For example, 666 morphological features, including all time-point data at 8-h intervals were initially used, then the dataset was decreased to 342 features by increasing the time-point interval to 16-h, and so on. The detailed modeling process using ridge regression followed a previously described method (Hastie et al., 2009).

For each of the three types of parameter evaluations, four types of prediction models were constructed, which covered the two types of prediction goals and two types of modeling scenarios. The two types of prediction models were as follows: (i) D14_ALP model that aimed to predict the ALP activity value measured on 14th day from the preceding morphological features (days 1–14); and (ii) D21_Ca model that aimed to predict the calcium deposition value measured after an additional week of differentiation culture (day 21) from the previous week's morphological features (days 15–21).

For each model, two types of modeling scenarios were tested. In Scenario I, which is applied as a new patient modeling scheme, the prediction model does not use information from within the same lot of cells model training. For instance, when we examined 3 lots of hBMSCs with 18 samples per lot (54 samples in total), for each prediction output the prediction model was trained with 36 samples from 2 lots of cells (e.g., lots 1 and 2), and then used to predict performance of the 18 samples from the remaining lot (e.g., lot 3). This scenario was designed to provide the advantage of performing an accurate cell quality evaluation from a newly accepted patient using historical data collected from other patients' cells. In Scenario II, the ongoing patient approach, a model is built by incorporating early data derived from the patient's own cells into the training set. For example, when using data from 54 samples consisting of 3 lots of hBMSCs, the prediction model is trained with 42 samples consisting of 2 lots (e.g., lots 1 and 2), plus 6 early samples from the remaining lot (e.g., images from the first passage of lot 3), and then predicts the remaining 12 samples. This scenario was designed to take advantage of early data that may be generated when cell therapy requires more than two passages to expand cells in order to obtain therapeutically relevant cell numbers. This scenario makes use of stored information obtained from previous patients plus the patient's own cellular morphology data, which can be used to predict the future quality of a newly accepted patient's cells.

We calculated standardized error as a metric for evaluating the performance of the prediction models as follows:

$$E_{\mathrm{ave}} = \sum_{k=0}^{N} (y_{\mathrm{p}} - y_{\mathrm{t}})^2 \tag{1}$$

$$E_{\mathrm{std}} = \frac{E_{\mathrm{ave}}}{V} \tag{2}$$

(E_{std}, standardized error; E_{ave}, averaged error; y_{p}, prediction value; y_{t}, teacher signal value; N, sample number; V, variance of all samples)

Performance is considered to be improved with a decrease in the standardized error. When the standardized error equals 1, the prediction yields are essentially equal to the average value for all test samples, which is equivalent to random guessing.

Results

Effect of Time-Course Length for the Prediction of Osteogenic Differentiation Potential Based on Image Data

We evaluated the performance of models derived from "shortening type" of dataset characterization to first determine the effect of morphological data acquisition period on predicting osteogenic differentiation potential (Fig. 2).

For both modeling scenarios, the prediction performance of the D14_ALP models were found to be high (standardized error < 0.5) for all models lacking morphology information collected after 40 h from start of induction (Fig. 2a).

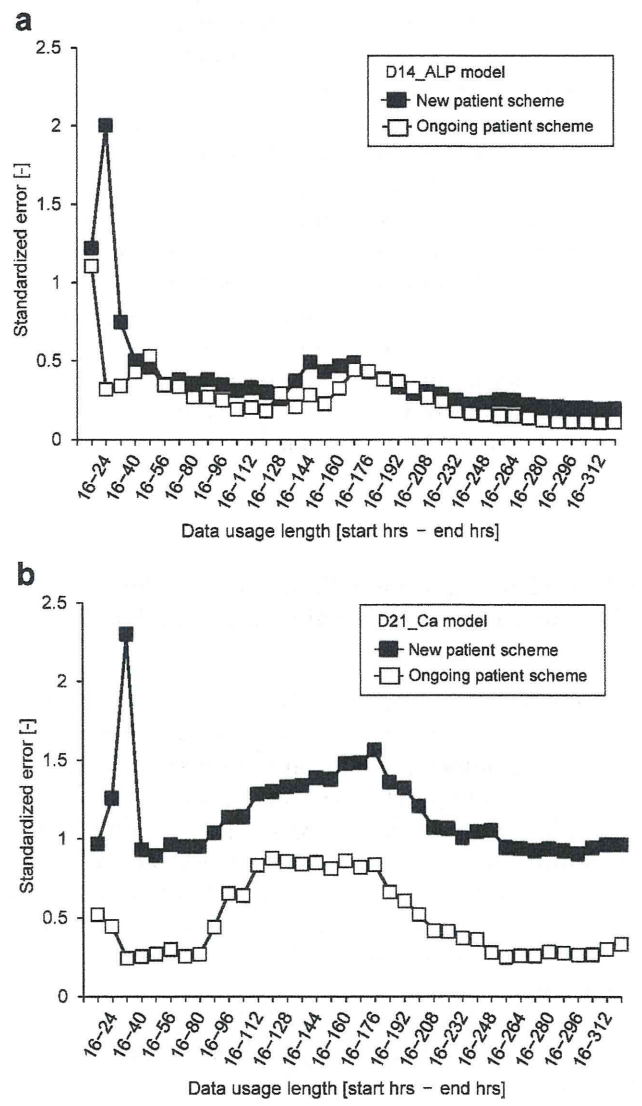

Figure 2. Prediction performance of shortening type use of morphological features. **a**: Performance of D14_ALP models. **b**: Performance of D21_Ca models. Filled squares and solid line, modeling with scenario I (new patient modeling); open squares and solid line, modeling with scenario II (ongoing patient modeling).

Surprisingly, in spite of the differences between construction scenarios, the prediction model using only morphological features from the first 2 days (precisely, 16–40 h) showed similar performance compared to the model using all information from the entire collection period. We have previously reported our scenario II to be the most effective modeling scenario by using all 14 days of morphological features. However, based on results from the present study, the scenario II-based models can reduce their data usage to only 8 h of data (16–24 h), which is sufficient to predict ALP activity after 14 days (Matsuoka et al., 2013). Considering aspects that have the greatest influence on diminishing performance, the scenario I-based models shifted performance drastically, when the morphological information from time-point 4 (40 h after the induction start) was removed, or when morphological features were limited to the very first day.

For D21_Ca models (Fig. 2b), we identified an observation time period that contributes uncertainty to the models. When morphological data from the culture period spanning 88–248 h is included in the model, we observe a noticeable decrease in model prediction accuracy. In contrast, features which cover only 48 h were found to construct models with consistent performance compared to the model using data from the entire sampling period (Fig. 2b). With D21_Ca, the difference in model between the two construction scenarios was marked. Our proposed approach with scenario II greatly enhanced performance of predicting further biological response after differentiation. Eight hours (16–24 h) of morphology measurements was also found to be sufficient to predict calcium deposition rate after 21 days of differentiation, which is similar to the findings when using D14_ALP models.

Effect of Image Collection Period Interval Within a Time-Course for Prediction of Osteogenic Differentiation Potential

The "window-shift type" of dataset characterization was evaluated to examine the critical time interval during which morphological information should be collected for the most accurate osteogenic differentiation model construction (Fig. 3). In our previous investigations, we found that a collection interval of approximately 2 days was sufficient to predict cellular quality (Sasaki et al., 2013); therefore, we set the size of the window to cover 2 days (6 time-points) and evaluated the effects of various 2 days intervals shifted over a total span of 14 days.

With a window-shift type of evaluation, we found that small numbers of morphological features gave stable and high prediction performance in D14_ALP models for most of the intervals tested. In contrast, D21_Ca model performances were poor in all intervals. Interestingly, we observed no significant differences in performance between scenarios I and II with the morphological features obtained from the 2 days period.

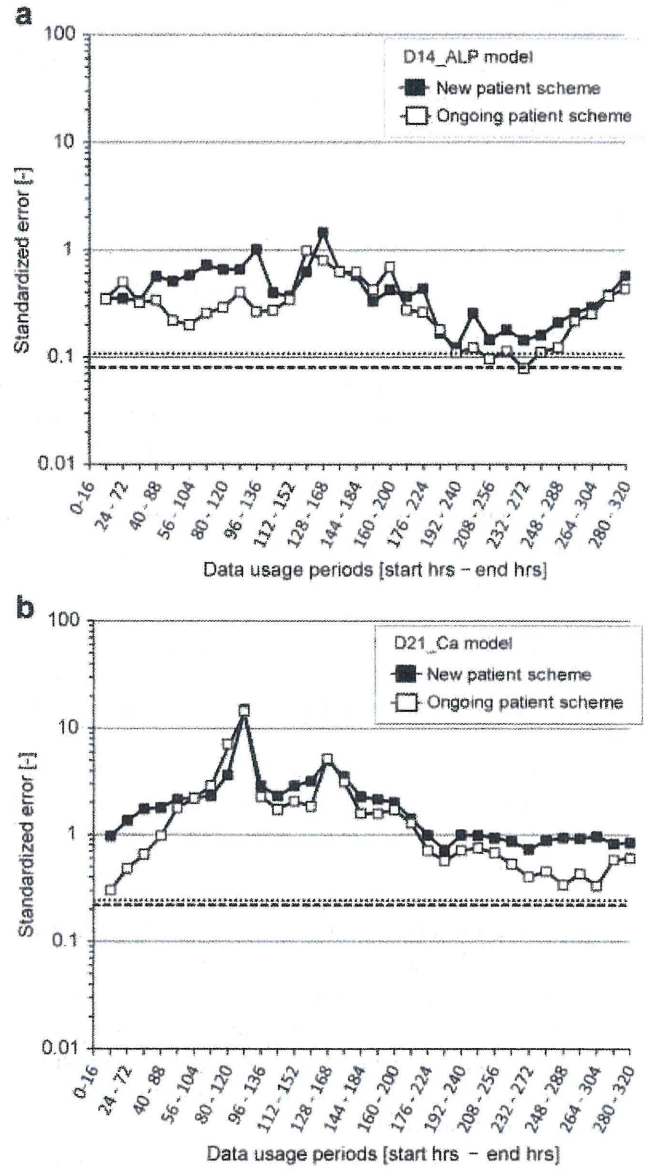

Figure 3. Prediction performance of window-shift type use of morphological features. **a**: Performance of D14_ALP models. **b**: Performance of D21_Ca models. Filled squares and solid line, modeling with scenario I (new patient modeling); open squares and solid line, modeling with scenario II (ongoing patient modeling). Dotted line, the lowest prediction error in Shortening type use of features; broken line, the lowest prediction error in Skipping type use of features. The axis indicating standard error is plotted in logarithmic scale for indicating a wider range of plots.

Effect of Image Data Sampling Frequency for Time-Course Prediction of Osteogenic Differentiation Potential

We evaluated the performance of models derived from "skipping type" data set characterization to explore the effect of image data density that would be sufficient for constructing accurate osteogenic differentiation models (Fig. 4). Starting with 8-h intervals from time-point 1 to 37, we decreased the frequency of image data collection, or

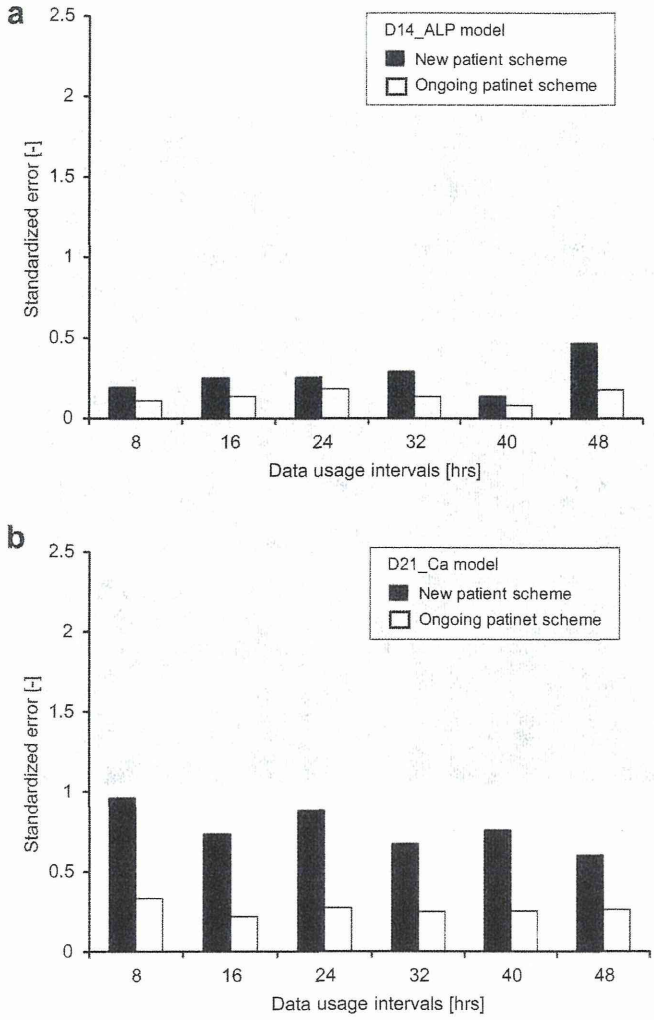

Figure 4. Prediction performance of skipping type use of morphological features. **a**: Performance of D14_ALP models. **b**: Performance of D21_Ca models. Filled bars, modeling with scenario I (new patient modeling); open bars, modeling with scenario II (ongoing patient modeling).

"skipped" interim time-points, which diminished the density of the overall dataset.

With D14_ALP models, prediction performance was nearly the same when using either 8- or 40-h sampling frequencies. Forty-eight hours sampling frequency was also found to be sufficient for clinical use. Scenario II constructed D21_Ca models also produced very highly accurate predictions using 48-h intervals. In contrast to the influence "skipping" data had in the D14_ALP models, the performance of D21_Ca models was enhanced by reducing the frequency of morphological features to 48-h intervals.

Discussion

To advance our previous findings, which proposed an automated approach for morphology-based prediction of osteogenic differentiation potential, we provide here a detailed critical evaluation of the image sampling requirements for morphological features of hBMSCs. Although an image-based cell quality assessment method provides greater advantages for industrialization of regenerative medicine due to its non-destructive nature, we designed this study to identify the critical morphological image sampling characteristics that would allow a resource-efficient prediction of osteogenic differentiation potential. Our focus was to balance accuracy, which can also be considered the prediction performance when only using microscopic images only, together with resource sparing, which considers the effort and expense required for its implementation. Thus, this study focused on reducing the resource demands of introducing our proposed cell quality prediction method in medical facilities that have to continuously run their current therapies without introduction of expensive hardware for automated image-acquisition. At the same time, we wanted to define the critical timing and number of morphological features that quantitatively allows detection of loss of hBMSC differentiation potential. In this study we reduced the data needed to be extracted from morphological features in order to predict both ALP activity (day 14) and calcium deposition rate (day 21) as compared to our previous report, in which we used a total of 666 morphological features (18 morphological features measured at 37 time-points, covering 14 days of differentiation culture) (Fig. 1).

Among all parameter reduction investigations, we found that modeling under scenario II (ongoing patient scenario) invariably provided better performance in both D14_ALP and D21_Ca models, compared to that under scenario I (new patient scenario). The strong performance of scenario II in this study was consistent with findings from our previous study and attributed to inclusion of the test patient's morphological data into the model. The present study also clarified that the weaker performance of scenario I models is not caused by improper use of morphological features, such as including a particularly noisy time-period or bias from overrepresentation of non-informative periods. We can now conclude more strongly that strong prediction performance of both ALP levels and calcium deposition can be achieved by following our scenario II modeling concept and focus further discussion only on scenario II modeling results.

From the performance of "shortening type" models (Fig. 2), we found that the minimum image-acquisition period could be shortened to the first 40 h after differentiation (standardized error < 0.5) in both D14_ALP and D21_Ca models. With a standardized error of 0.5, this prediction model is nearly twofold better than random guessing. It was surprising to find that the biochemical measurements of osteogenic differentiation after 2–3 weeks of culturing can be identified by morphological changes seen within the first 2 days. This finding indicates that a differentiation quality check of hBMSCs can be performed in a very early period, so that additional unnecessary culturing can be reduced.

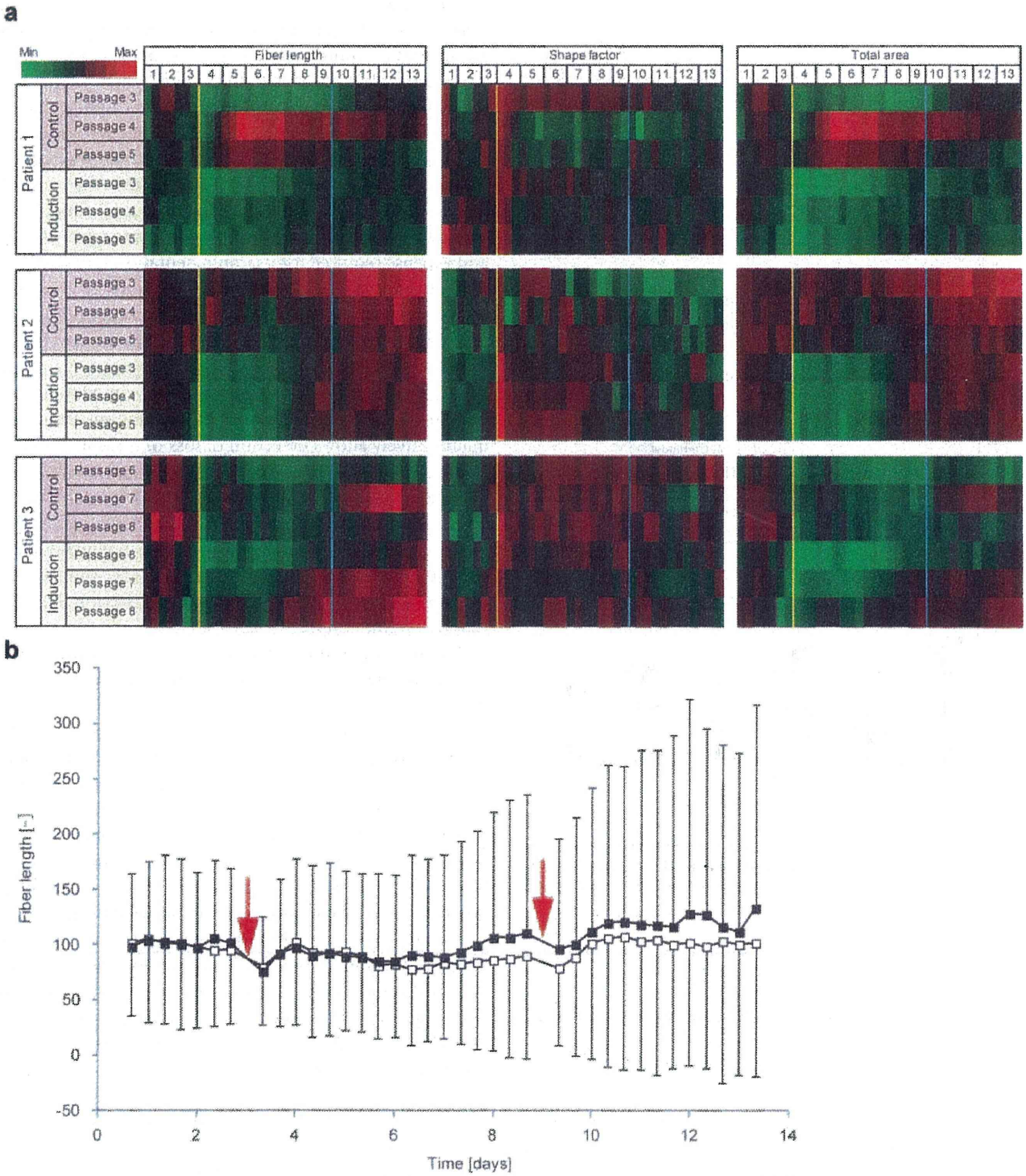

Figure 5. Responses of morphological features to medium change events. Typical responses that appear in morphological features in all lots (**a**) and in Lot 1 (**b**) are shown as representative examples. (a) Heat map of morphological features (fiber length, shape factor, and total area) were shown with red (maximum) and green (minimum). Each square was colored based on the mean value of each morphological feature from all cells under 1 condition (3 wells × 5 view fields). Roughly, 4,000–40,000 cells were measured to obtain this mean value. (b) Longitudinal changes in average of Fiber length over time. Filled square, control samples; open square, induction samples. All average values were calculated as for Fig. 5a. Error bars indicate standard deviation. Red arrows indicate the timing of medium changes.

The "window-shift type" model evaluation revealed a critical period for obtaining the most informative morphological features (Fig. 3). When attempting prediction with only 108 features (i.e., 16% of the information compared to that used in our original study), we found that the morphological changes in culture days 8–10 (D14_ALP model) and days 9–11 (D21_ALP model) are most informative and enhance prediction performance. This result largely matched the performance of "skipping type" models (Fig. 4). Most "skipping type" models exceeded the performance of models from the later stages in the "shortening type" analyses, which lost predictive strength in this portion of the time-course. The lack of later-stage morphological features correlated with decreased prediction performance in both D14_ALP and D21_Ca models, but more so in D21_Ca models, when derived from "shortening type" evaluations. This suggests morphological changes are informative in the first 2 days, but incorporation of morphological features from later stages of differentiation can further improve prediction accuracy. From this observation we conclude that acquiring additional images from the later stages of differentiation culture are not essential, but can add value to prediction models. Considering both observations from "shortening type" and "skipping type" evaluations, we conclude the image-acquisition from the first 2 days of a "shortening type" model, can be reduced by loosening the image acquisition schedule to a frequency of 48 h intervals without significant impact to correctly classifying candidate differentiation potential. An advantage to widening the sampling frequency to 48 h intervals is the ability to implement a manual version of this method in a clinical setting that frees up weekend time and mitigates resource burden on operators and facilities.

We also identified limitations of the morphological features reflecting cellular potential. As shown in Figure 4, the "shortening type" analysis revealed that including changes in morphological features from the first day (16–32 h) undermines the prediction performance. These observations suggest morphological changes in the first day of differentiation culture are likely more random compared to subsequent changes in morphology that more directly contribute to prediction of osteogenic potential. Since cells had attached sufficiently during the expansion culture period in the same plate wells prior to day 0 in our experiment, these extraordinary morphological changes are likely a response to changing the culture environment to differentiation medium. We therefore further examined the morphological responses to medium changes (Fig. 5). When the differentiation period started, medium was changed at 64 h (day 3) and at 216 h (day 10; Fig. 5a). Surprisingly, many morphological features showed irregular changes after the medium was refreshed, which we interpret as clear morphological responses to the medium change. When viewed collectively these morphological responses to medium change were limited to particular morphological features. The morphological parameter, "fiber lengths," was one parameter sensitive to medium changes (Fig. 5b). Even though these changes were small from a statistical point of view, this parameter, which indicates cell shrinkage, was most sensitive to medium change across all cell lots. Although most of these features were insensitive to the second medium change at time-point 26, fiber length still reflected this change in the environment. We found a drift in model performance in the "shortening type" and "window-shift type" analyses, which was due to parameter disturbances reflecting this response to medium change. Based on our observations we suggest correcting for these types of morphological parameters, which may be a source of noise when used in predictions of cellular ostogenic potential. This finding also strongly indicates the possibility that cellular morphology changes can also be used to detect changes in cellular microenvironment as a way to quality check animal cells during high-throughput assays.

The utility of morphology-based cell quality evaluation has also been studied by Seiler et al. where they reported a systematic evaluation method for hBMSCs' differentiation potential based on morphological features measured from non-labeled time-course images (Seiler et al., 2012). Building on the work of Seiler et al. and their algorithm approach (node-harvest method), our original report greatly expands the utility of the image-based modeling concept by advancing the field in three areas: (i) improved model performance by data accuracy, (ii) various modeling scenarios for practical implementation in clinics, and (iii) quantitative prediction of osteogenic potential (versus classifications). The further iterations presented here add three more advancements: (i) identification of a critical period for measuring morphological features, (ii) the sensitivity of particular morphological features, and (iii) the most resource-efficient data collection method.

In conclusion, in this study, we were able to define the key characteristics of hBMSC morphological features to advance our image-based computational prediction model. The detailed characterization of morphological features in this study has demonstrated a way that allows practical, flexible and efficient introduction of our method, allowing users to most appropriately match facilities and protocols. Our next investigation to universalize this application should be the confirmation of our method under different imaging platforms. We believe that this is a benchmark study highlighting the importance of real-time morphological features for use in prediction modeling, which may trigger wider implementation of this approach to address the need for cell quality evaluation methods in regenerative medicine.

We are grateful to the New Energy and Industrial Technology Development Organization (NEDO) for the Grant for Industrial Technology Research (Financial Support to Young Researchers, 09C46036a) for financial support. We also thank Mai Okada and Yurika Nonogaki for help with experiments and data storage. We are deeply grateful to Wakana Yamamoto, Yoshihide Nagura, Kazuhiro Mukaiyama, Kenji Kojima, Hiroto Sasaki, and Asuka Miwa for establishing the basic analysis protocol and algorithms for the image analysis procedure.

References

Becker T, Madany A. 2012. Morphology-based features for adaptive mitosis detection of in vitro stem cell tracking data. Methods Inf Med 51(5):449–456.

Erdmann G, Volz C, Boutros M. 2012. Systematic approaches to dissect biological processes in stem cells by image-based screening. Biotechnol J 7(6):768–778.

Hastie T, Tibshirani R, Friedman J. 2009. The elements of statistical learning: Data mining, inference, and prediction. New York, NY: Springer Science+Business Media. pp 43–94.

Hong L, Peptan IA, Xu H, Magin RL. 2006. Nondestructive evaluation of osteogenic differentiation in tissue-engineered constructs. J Orthop Res 24(5):889–897.

Kagami H, Agata H, Tojo A. 2011. Bone marrow stromal cells (bone marrow-derived multipotent mesenchymal stromal cells) for bone tissue engineering: Basic science to clinical translation. Int J Biochem Cell Biol 43:286–289.

Kino-Oka M, Maeda Y, Sato Y, Maruyama N, Takezawa Y, Khoshfetrat AB, Sugawara K, Taya M. 2009. Morphological evaluation of chondrogenic potency in passaged cell populations. J Biosci Bioeng 107:544–551.

Li W, Hong L, Hu L, Magin RL. 2010. Magnetization transfer imaging provides a quantitative measure of chondrogenic differentiation and tissue development. Tissue Eng Part C Methods 16C(6):1407–1415.

Matsuoka F, Takeuchi I, Agata H, Kagami H, Shiono H, Kiyota Y, Honda H, Kato R. 2013. Morphology-based prediction of osteogenic differentiation potential of human mesenchymal stem cells. PLoS ONE 8(2): e55082.

Maul TM, Chew DW, Nieponice A, Vorp DA. 2011. Mechanical stimuli differentially control stem cell behavior: morphology, proliferation, and differentiation. Biomech Model Mechanobiol 10(6):939–953.

Platt MO, Wilder CL, Wells A, Griffith LG, Lauffenburger DA. 2009. Multipathway kinase signatures of multipotent stromal cells are predictive for osteogenic differentiation: tissue-specific stem cells. Stem Cells 27(11):2804–2814.

Poirier-Quinot M, Frasca G, Wilhelm C, Luciani N, Ginefri JC, Darrasse L, Letourneur D, Le Visage C, Gazeau F. 2010. High-resolution 1.5-Tesla magnetic resonance imaging for tissue-engineered constructs: a noninvasive tool to assess three-dimensional scaffold architecture and cell seeding. Tissue Eng Part C Methods 16C(2):185–200.

Ratcliffe A. 2011. The translation of product concept to bone products: A partnership of therapeutic effectiveness and commercialization. Tissue Eng B 17B(6):443–447.

Sasaki H, Matsuoka F, Yamamoto W, Kojima K, Honda H, Kato R. 2013. Image-based cell quality assessment: Modeling of cell morphology and quality for clinical cell therapy, studies in mechanobiology. Tissue Eng Biomater 10:207–226.

Seiler C, Gazdhar A, Reyes M, Benneker LM, Geiser T, Siebenrock KA, Gantenbein-Ritter B. 2012. Time-lapse microscopy and classification of 2D human mesenchymal stem cells based on cell shape picks up myogenic from osteogenic and adipogenic differentiation. J Tissue Eng Regen Med 19: doi: 10.1002/term.1575.

Smith DM. 2012. Assessing commercial opportunities for autologous and allogeneic cell-based products. Regener Med 7(5):721–732.

Unadkat HV, Groen N, Doorn J, Fischer B, Barradas AM, Hulsman M, van de Peppel J, Moroni L, van Leeuwen JP, Reinders MJ, van Blitterswijk CA, de Boer J. 2012. High content imaging in the screening of biomaterial-induced MSC behavior. Biomaterials 34(5):1498–1505.

Wang W, Deng D, Li J, Liu W. 2013. Elongated cell morphology and uniaxial mechanical stretch contribute to physical attributes of niche environment for MSC tenogenic differentiation. Cell Biol Int 37(7):755–760.

Zhang D, Kilian KA. 2013. The effect of mesenchymal stem cell shape on the maintenance of multipotency. Biomaterials 34(16):3962–3969.

TISSUE ENGINEERING: Part A
Volume 20, Numbers 7 and 8, 2014

DOI: 10.1089/ten.tea.2013.0333

Stage-Specific Embryonic Antigen 4 in Wharton's Jelly–Derived Mesenchymal Stem Cells Is Not a Marker for Proliferation and Multipotency

Haiping He, MD,[1–3] Tokiko Nagamura-Inoue, MD, PhD,[2] Hajime Tsunoda, MD, PhD,[4] Miki Yuzawa, MT,[2] Yuki Yamamoto, MT,[2] Pariko Yorozu, BNS,[2] Hideki Agata, PhD,[5] and Arinobu Tojo, MD, PhD[1,2]

Background: Umbilical cord Wharton's jelly (WJ) is a rich source of mesenchymal stem cells (MSCs) similar to bone marrow (BM) and adipose tissues. Stage-specific embryonic antigen (SSEA)4 has been reported as a stem cell marker in BM-derived MSCs, but whether $SSEA4^+$ cells have growth and differentiation advantages over $SSEA4^-$ cells remains controversial. To gain insight into the role of SSEA4, we studied $SSEA4^+$ cells in WJ-derived MSCs (WJ-MSCs).

Methods: WJ-MSCs were collected by the explant (WJe-MSCs) or collagenase methods (WJc-MSCs) and analyzed by flow cytometry and reverse-transcription polymerase chain reaction (RT-PCR). To evaluate whether culture conditions influenced the SSEA4 expression, WJe-MSCs were cultured in the medium supplemented with different fetal bovine serum (FBS) concentrations.

Results: SSEA4 was expressed for a long-term culture. In contrast, $SSEA3^+$ disappeared rapidly in early passages of the culture. The incidence of $SSEA4^+$ and $SSEA3^+$ cells was similar between WJe-MSCs and WJc-MSCs at passages P0–P9, except for transient depletion of SSEA4 expression in early passages of WJe-MSCs. These were $CD73^+CD105^+$ cells that express embryonic stem cell markers detected by RT-PCR. No differences in growth and differentiation ability of osteocytes and adipocytes were observed between the sorted $SSEA4^+$ cells and $SSEA4^-$ cells. Further, SSEA4 expression in WJe-MSCs was significantly correlated with FBS concentration in the culture medium.

Discussion: SSEA4, which may display altered expression profiles in response to culture conditions, may not be an essential marker of WJ-MSC multipotency.

Introduction

Umbilical cord (UC) Wharton's jelly (WJ) is a rich source of mesenchymal stem cells (MSCs) along with bone marrow (BM) and adipose tissue.[1–3] WJ-derived MSCs (WJ-MSCs) exhibit the characteristics of MSCs as defined by the International Society for Cellular Therapy (ISCT) criteria. First, MSCs are plastic adherent when maintained in standard culture conditions; second, they are positive for CD105, CD73, HLA-class I, and CD90 and negative for CD45 and HLA-DR surface molecules; and third, MSCs have the pluripotent ability of various mesoderm lineages to generate adipocytes, osteoblasts, and chondrocytes.[4,5] Similar to BM-derived MSCs (BM-MSCs), WJ-MSCs have the potential to differentiate into mesoderm-derived tissues, endoderm, and ectoderm lineages, such as endothelial cells, cardiac myoblasts, pancreatic cells, hepatocytes, and neurogenic cells.[6,7] Hsieh *et al.* compared the gene expression profiles of BM-MSCs and WJ-MSCs and reported that WJ-MSCs were more primitive and more similar to embryonic stem (ES) cells than BM-MSCs.[8,9] On the basis of this data, we isolated the primitive MSCs in WJ-MSCs that are similar to ES cells. Markers of pluripotent, undifferentiated ES cells express several nuclear transcription factors, such as *Oct4, Nanog*, and *SOX2*, and cell surface antigens that have been used to define ES cells, including stage-specific embryonic antigen (SSEA)3 and

[1]Division of Molecular of Therapy, Center for Advanced Medical Research, The Institute of Medical Science, The University of Tokyo, Tokyo, Japan.
[2]Department of Cell Processing and Transfusion, The Institute of Medical Science, The University of Tokyo, Tokyo, Japan.
[3]Department of Hematology, First People Hospital of Yunnan Province, Kunming, China.
[4]Department of Obstetrics, NTT Medical Center Tokyo Hospital, Tokyo, Japan.
[5]Tissue Engineering Research Group, Division of Molecular Therapy, The Institute of Medical Science, The University of Tokyo, Tokyo, Japan.

4. The latter two cell surface antigens are present on human ES cells and human embryonic carcinoma cells and are downregulated as these cells differentiate. SSEA3 and SSEA4 are epitopes on the related glycosphingolipids (GSLs), GL-5 and GL-7, respectively. GSLs consist of a carbohydrate moiety or a chain linked to ceramide[10] and appear to be attractive surface markers for sorting live ES-like primitive cells from WJ-MSCs. However, the role of SSEA3 and SSEA4 as pluripotent markers remains controversial, with different laboratories reporting variable results. Gang *et al.* reported that SSEA4 is a marker for BM-MSCs,[11] and Wakao *et al.* showed that SSEA3 is a pluripotent stem cell marker on MSCs defined as multilineage-differentiating stress-enduring (Muse) cells.[12,13] In contrast, Brimble *et al.* demonstrated that both SSEA3 and SSEA4 are not essential for human ES cell pluripotency, as proven by GSL inhibitors.[14]

To obtain $SSEA3^+/4^+$-rich MSCs, we compared the following two major collection methods from the UC: the explant method (WJe-MSCs) and the collagenase-treatment method (WJc-MSCs). We previously reported that WJe-MSCs by the explant method were preferred over that by the collagenase method because WJ-MSCs treated with collagenase sometimes showed decreased cell viability due to the lytic activity of collagenases. However, we could not determine whether the cells migrating from the tissue in the explant method could be selected and induced to differentiate to some degree.

In this study, we compared SSEA3/4 expression in WJ-MSCs collected by different methods. To examine the potential role of SSEA4 in WJ-MSCs, we studied the growth and differentiation ability of cells sorted by SSEA4 expression and factors that influence its expression.

Materials and Methods

Isolation and culture of adherent cells

The present study was approved by the Ethics Committee of the Institute of Medical Science, University of Tokyo, Japan, and the NTT Medical Center Tokyo hospital. Informed consent was obtained from mothers planning to have cesarean sections. UCs were collected aseptically from full-term cesarean section patients after informed consent. The UCs were transferred after collection and the process was initiated within 24 h of delivery. The UC surface was rinsed with phosphate-buffered saline (PBS; Gibco–BRL) containing antibiotics and antifungal reagents Anti–Anti (Antibiotic–Antimycotic, 100×; Gibco–BRL). After removing two arteries and one vein, the remaining WJ tissues were minced into 1–2 mm^3 fragments and divided into two groups for the explant and collagenase-treatment methods (Fig. 1A). In the explant method, the minced fragments were aligned and attached at regular intervals in 10-cm culture dishes. After the fragments were semi-dried and firmly attached to the bottom, the culture medium was gently poured into the dishes.[1,15] In the collagenase-treatment group, the minced WJ tissues were incubated in 1 mg/mL collagenase type I solution (Sigma–Aldrich) in α-MEM (Gibco–BRL) with shaking at 37°C for 2–3 h.[15,16] The cells were then washed with α-MEM supplemented with 10% fetal bovine serum (FBS) and seeded in 10-cm tissue culture dishes with the culture medium as described earlier.[1] The culture medium was refreshed once a week for 3–4 weeks until fibroblast-like adherent cells reached 80–90% confluence. The first-harvested master cells were defined as passage 0 (P0; Fig. 1B). The adherent cells and tissue fragments (Fig. 1A) were rinsed once with PBS and detached using 10% trypsin solution (TrypLE Express; Invitrogen) followed

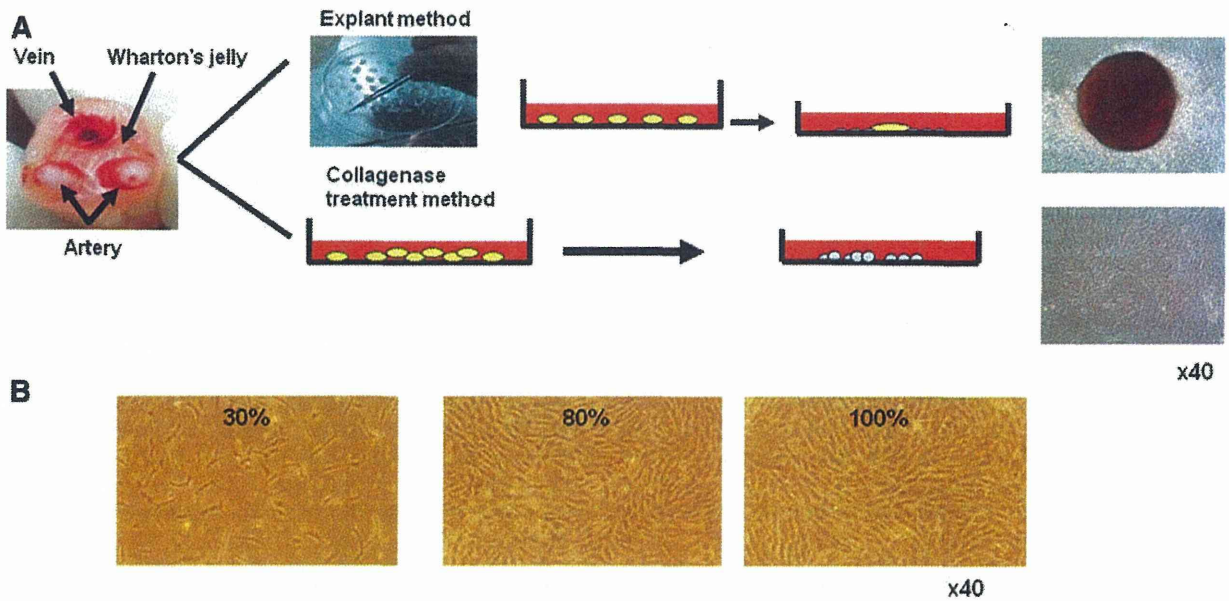

FIG. 1. Umbilical cord Wharton's jelly–derived mesenchymal stem cells (WJ-MSCs). **(A)** MSCs were collected from umbilical cord WJ tissue by the explant method (WJe-MSCs) and by the collagenase-treatment method (WJc-MSCs). Photographs of migrating cells from the minced tissue in the explant method and adherent cells from the scattered cells in the collagenase-treatment method are shown. **(B)** Both WJe-MSCs and WJc-MSCs were spindle-shaped fibroblast-like cells. Color images available online at www.liebertpub.com/tea

by washing with α-MEM supplemented with 10% FBS. In the explant method, the cells and tissue fragments were filtered to remove the tissue fragments. The harvested cells, other than those undergoing further analysis, were immediately cryopreserved in 10% DMSO/5% dextran 40 solution. For serial cultures, the cells were inoculated at 2×10^5 cells per 10-cm-diameter dish and counted at each passage.

Flow cytometry analysis and sorting

Standard flow cytometry (FCM) techniques were used to determine the typical cell surface markers of WJ-MSCs. WJ-MSCs were stained with the following mouse monoclonal antibodies (mAbs): phycoerythrin (PE)–conjugated anti-human CD73 (BD), CD271 (Miltenyi), and HLA-ABC (BD); fluorescein isothiocyanate (FITC)–conjugated anti-human CD90 (BD), CD105 (eBioscience), HLA-DR (BD), and CD45 (BD), FITC-, PE-, and Alexa Fluor–conjugated anti-mouse IgGs (BD) were used as isotypic controls. Dead cells were identified by staining with propidium iodide. To detect the ES cell markers in WJ-MSCs, Alexa Fluor–conjugated mouse anti-human SSEA4 (Clone MC813-70; BD) and FITC-conjugated rat anti-human SSEA3 (Clone MC631; BD) together with the MSC markers CD73 or CD105 mAbs were used. The stained cells were acquired with an FACSCaliber (BD) and analyzed by FlowJo (Tomy Digital Biology, Co. Ltd.). For cell sorting, WJe-MSCs were stained with Alexa-conjugated anti-human SSEA4 and PE-conjugated anti-human CD73 antibodies. The cells were acquired with an FACSAria cell sorting system (BD) and sorted by SSEA4, SSEA3, and CD73 expression.

Proliferation assays of sorted SSEA4$^+$ and SSEA4$^-$ MSCs

To evaluate the proliferative abilities of sorted SSEA4$^+$ and SSEA4$^-$ WJe-MSCs, the sorted cells were plated at 1×10^4/well in six-well plates (Greiner Bio-one) and cultured in α-MEM supplemented with 10% FBS. The cells were harvested every week and the cell numbers were counted with trypan blue (Gibco–BRL) for 9 weeks.

SSEA4 expression in WJ-MSCs with different FBS concentrations

To evaluate whether culture conditions influenced the SSEA4 expression, WJe-MSCs (P0) were cultured at 1×10^5 cells/well in six-well plates ($n=3$) in α-MEM with the indicated FBS concentrations. After 1 week, the SSEA4, SSEA3, and CD73 expression was analyzed by FCM. To study the influence of the proliferation of WJe-MSCs on SSEA4 expression, we explored the time-course experiment to see the relationship between SSEA4 expression and WJe-MSC growth curve. WJe-MSCs were plated in six-well plates with indicated concentrations of FBS, and the cell number was counted to figure the growth curve on indicated days. The cells were analyzed by FCM to analyze the expression of SSEA3, SSEA4, and CD73.

Further, to analyze the influence of FBS on SSEA4$^-$ WJe-MSCs, SSEA4$^+$ and SSEA4$^-$ WJe-MSCs were cultured in 12-well plates with different concentrations of FBS followed by FCM.

SSEA4 expression in BM-MSCs with different FBS concentrations

To clarify that the phenomena of SSEA4 expression are limited to the WJe-MSCs, we studied the SSEA4 expression in BM-MSCs obtained from BM mononuclear cells (MNCs). Frozen BM-MNCs were purchased from Lonza Walkersville, Inc. BM-MNCs (8×10^5/well) were seeded in six-well plates and grown at 37°C with 5% CO_2. On days 0–21, the proportion of CD45-, SSEA4-, and CD73-positive or -negative cells were analyzed by FCM. To see the influence of FBS on BM-MSCs, we continued to culture BM-MNCs in α-MEM supplemented with 10% FBS and obtained the MSCs. BM-MSCs at p2 were plated in six-well plates to figure the growth curve and analyzed the incidence of CD45, SSEA3, SSEA4, and CD73 by FCM, as described in WJe-MSCs.

RNA isolation and reverse-transcription polymerase chain reaction analysis

Total RNAs were extracted from WJ-MSCs at P3 and from sorted SSEA4$^+$ and SSEA4$^-$ MSCs using TRIzol® Reagent (Invitrogen Corp.). Reverse-transcription polymerase chain reaction (RT-PCR) was performed using the PrimeScript RT-PCR Kit (Takara Shuzou) according to the manufacturer's instructions. The ES markers *Nanog*, *Oct4*, *Klf4*, and *Sox2*[17] and *glyceraldehyde-3-phosphate dehydrogenase* (GAPDH) as the control were amplified from the synthesized cDNAs by PCR with the primer pairs shown in Table 1. The amplification conditions were 35 cycles of denaturation at 94°C for 30 s, annealing at 56°C for 30 s, and

TABLE 1. HUMAN PRIMER SEQUENCES USED FOR REVERSE-TRANSCRIPTION POLYMERASE CHAIN REACTION

Gene	*Accession*		*Primer sequence*	*Product size (bp)*
hOCT3/4	NM-002701	Sense	5′ GACAGGGGGAGGGGAGGAGCTAGG 3′	144
		Anti-sense	5′ CTTCCCTCCAACCAGTTGCCCCAAAC 3′	
REX1	NM-174900	Sense	5′ CAGATCCTAAACAGCTCGCAGAAT 3′	306
		Anti-sense	5′ GCGTACGCAAATTAAAGTCCAGA 3′	
NANOG	NM-024865	Sense	5′ CAGCCCCGATTCTTCCACCAGTCCC 3′	391
		Anti-sense	5′ CGGAAGATTCCCAGTCGGGTTCACC 3′	
hSOX2	NM-003106	Sense	5′ GGGAAATGGGAGGGGTGCAAAAGAGG 3′	151
		Anti-sense	5′ TTGCGTGAGTGTGGATGGGATTGGTG 3′	
hKLF4	NM-004235	Sense	5′ ACGATCGTGGCCCCGGAAAAGGACC 3′	397
		Anti-sense	5′ TGATTGTAGTGCTTTCTGGCTGGGCTCC 3′	
hGAPDH	NM-002046	Sense	5′ AACAGCCTCAAGATCATCAGC 3′	338
		Anti-sense	5′ TTGGCAGGTTTTTCTAGACGG 3′	

extension at 72°C for 1 min. The PCR products were separated by electrophoresis on 2.0% agarose gels and visualized by staining with ethidium bromide.[1]

Adipogenic differentiation

WJe-MSCs were cultured at 2×10^4 cells/well in six-well plates in α-MEM supplemented with 10% FBS. When the cells achieved 80% confluence, the medium was replaced with adipogenesis induction medium,[8] consisting of 100 μM indomethacin (Sigma–Aldrich), 1 μM dexamethasone (Sigma–Aldrich), 0.5 mM IBMX (Sigma–Aldrich), and 10 μg/mL insulin (Sigma–Aldrich). The medium was refreshed every 3 days. After 3 weeks, the cells were fixed with 10% formaldehyde, washed with PBS and 60% isopropanol, and stained with Oil Red O (Sigma–Aldrich).

Osteogenic differentiation

WJe-MSCs at 2×10^4/well (P2) and SSEA4$^+$ and SSEA4$^-$ WJe-MSCs were cultured in 24-well plates in α-MEM supplemented with 10% FBS. On the following day, the medium was replaced with osteogenic induction medium including 10 nM dexamethasone (Sigma–Aldrich), 10 mM β-glycerol phosphate (Sigma–Aldrich), 100 μM ascorbic acid (Sigma–Aldrich), and 50 ng/mL human BMP2 (rhBMP2; Peprotech).[18,19] Human-BM-derived MSCs were used as the positive control. The induction medium was refreshed every 3 days. After 5 weeks, the cells were fixed with 2.5% glutaraldehyde for 15 min at room temperature followed by rinsing with PBS. The bone matrix was stained with 2% Alizarin Red S solution (Sigma–Aldrich) with pH adjusted to ~4.1–4.3 with 1% ammonium hydroxide (Sigma–Aldrich).[19]

Statistical analysis

Differences between groups were analyzed with JMP 6.0.2 software (SAS Institute). Statistical analyses were performed with Turkey–Kramer tests, and a p-value of 0.05 was regarded as statistically significant.

Results

Collection efficiency and WJe-MSC and WJc-MSC biomarkers

Both WJe-MSCs and WJc-MSCs were spindle-shaped fibroblast-like cells (Fig. 1B). There was no significant difference between these two methods in the collected cell numbers at P0, even though the collected cell numbers of WJe-MSCs varied (Fig. 2A). The median number of collected WJe-MSCs from 1 g of WJ was 2×10^6 (range, from 9.1×10^4 to 10.3×10^6; $n=23$) and of collected WJc-MSCs was 1.7×10^6 (range, from 9.2×10^4 to 7.5×10^6; $n=20$). Further, we compared their surface markers as defined by the ISCT. Both WJe-MSCs and WJc-MSCs were positive for CD73, CD90, CD105, and HLA-ABC with a small percentage of cells also positive for CD271 and negative for CD34, CD45, and HLA-DR (Fig. 2B). In addition, both WJe-MSCs and WJc-MSCs expressed the ES-related genes *Nanog*, *Oct4*, *Klf4*, *Rex1*, and *Sox2* (Fig. 2C).

Expression of SSEA4 and SSEA3 in WJ-MSCs

Because SSEA4$^+$ and SSEA3$^+$ cells have been considered as representative of immature cells, we periodically monitored SSEA4, SSEA3, and CD73 expression in WJe-MSCs and WJc-MSCs during P0–P9. The percentages of SSEA4$^+$ cells at P0 were similar in WJe-MSCs and WJc-MSCs. At P0, the WJe-MSCs included 32.4%±17.5% SSEA4$^+$CD73$^+$, 62.8%±18.9% SSEA4$^-$CD73$^+$, and 1.3%±1.8% SSEA4$^+$CD73$^-$, whereas the WJc-MSCs included 26.1%±16.1%, 70.4%±16.2%, and 0.7%±0.8% cells, respectively ($n=8$, $p=0.21$). However, the percentage of WJe-MSC SSEA4$^+$ cells decreased after the first passage and recovered to the original level by P7, whereas the incidence of WJc-MSC SSEA4$^+$ cells was relatively stable until P9 (Fig. 3A, C). In contrast, the percentage of SSEA3$^+$ cells among both WJe-MSCs and WJc-MSCs was highest at P0 that declined and disappeared by P5 (Fig. 3B, D). At P0, the percentage of SSEA3$^+$ cells among WJe-MSCs was 6.7%±6.3% and among WJc-MSCs was 6.1%±6.1% ($n=6$).

Comparison of SSEA4$^+$ and SSEA4$^-$ cells sorted from WJe-MSCs

Further, we sorted SSEA4$^+$ and SSEA4$^-$ cells from WJe-MSCs at P4 using FACSAria and analyzed the SSEA4 expression in the sorted cells every week. The mean purity of SSEA4$^+$CD73$^+$ was 89% and that of SSEA4$^-$CD73$^+$ was 97.7%. The SSEA4$^+$ MSCs and SSEA4$^-$ MSCs were of similar sizes (Fig. 4A).

The percentage of SSEA4$^+$ cells derived from the sorted SSEA4$^+$ WJe-MSCs decreased rapidly in the first week and then increased gradually until week 4 (Fig. 4B, C). Interestingly, SSEA4$^+$ MSCs were present in the SSEA4$^-$ WJe-MSCs, and the incidence of SSEA4$^+$ cells in the subsequent cultures was similar to that in the SSEA4$^+$-sorted cells. After week 4, the incidence of SSEA4$^+$ cells from both the SSEA4$^+$ and SSEA4$^-$ MSCs decreased to <10%. The incidences of SSEA4$^+$ cells derived from SSEA4$^+$ WJe-MSCs and SSEA4$^-$ WJe-MSCs were 8.5%±8.8% and 8.5%±8.8% at week 1 and 43.5%±21.6% and 55.1%±29.4% at week 4, respectively ($n=3$; Fig. 4C). In addition, there was no difference in proliferation ability between SSEA4$^+$ and SSEA4$^-$ WJe-MSCs (Fig. 4D).

RT-PCR analysis showed that the sorted SSEA4$^+$ and SSEA4$^-$ WJe-MSCs expressed *Nanog*, *Oct4*, and *Klf4* (Fig. 4E).

Adipocyte differentiation

To determine the differentiation ability of SSEA4$^+$ WJe-MSCs, we induced sorted SSEA4$^+$ and SSEA4$^-$ WJe-MSCs into adipocytes. With induction medium, we observed the accumulation of Oil Red O-stained lipid drops in SSEA4$^+$, SSEA4$^-$, and nonsorted WJe-MSCs, whereas there were no changes in WJe-MSCs cultured without induction medium (Fig. 5A).

Osteogenic differentiation

We also compared the osteogenic differentiation abilities of SSEA4$^+$ and SSEA4$^-$ WJe-MSCs. There was no difference between SSEA4$^+$ and SSEA4$^-$ WJe-MSCs after histochemical staining with Alizarin red, even though WJe-MSCs were difficult to differentiate into osteoblasts, as previously reported. Induction of osteogenic differentiation in WJe-MSCs required a relatively high concentration